Journal of Alloys and Compounds 503 (2010) 145–150

Contents lists available at ScienceDirect

Journal of Alloys and Compounds

journal homepage: www.elsevier.com/locate/jallcom

In situ reaction synthesis of Ti–TiB composites containing high volume fraction of TiB by spark plasma sintering process

Zhao-hui Zhang*, Xiang-Bo Shen, Sai Wen, Jie Luo, Shu-kui Lee, Fu-chi Wang

School of Materials Science and Engineering, Beijing Institute of Technology, Beijing, 100081, PR China

ARTICLE INFO

Article history:
Received 15 January 2010
Received in revised form 28 April 2010
Accepted 28 April 2010
Available online 5 May 2010

Keywords:
Ceramic–matrix composites
Microstructure
Mechanical properties
Spark plasma sintering

ABSTRACT

The *in situ* toughened Ti–TiB ceramic–matrix composites containing high volume fraction of TiB were synthesized by spark plasma sintering technique under a pressure of 50 MPa, with sintering temperature ranging from 1100 °C to 1400 °C and heating rate of 150 °C/min, using Ti and TiB_2 powders. Results indicated that Ti–TiB composites sintered at 1400 °C provided the optimal combination of dense microstructure, well developed lath-shaped TiB grains, and excellent mechanical properties, including the relative density of 99.6%, bending strength of 608 MPa, and a rather high fracture toughness of 9.35 MPa $m^{1/2}$. Moreover, the micro-hardness of the composites reaches a relatively high level (18.3 GPa).

1. Introduction

Spark plasma sintering (SPS), also known as the field-assisted sintering technique (FAST), is a comparatively novel sintering process that allows the compacted powders to be sintered at low temperatures, with short heating, holding, and cooling time compared to that used in conventional sintering technique [1–3]. In SPS process, raw powders in a graphite die are pressed uniaxially and a high-density pulsed direct current is applied, both the joule heating and the plastic deformation effects contribute to densification of the powders. Therefore, rapid heating is available and the bulk compacts with fine grain microstructure can be obtained [4–9]. Hence, SPS process is considered to be suitable for the fabrication of the hard-to-sinter materials such as ceramics, metal–ceramic composites, amorphous materials, nanocrystalline materials, and so on [10–13].

Titanium boride (TiB) and titanium diboride (TiB_2) ceramics exhibit an excellent combination of attractive physical and mechanical properties such as high hardness, low density, good corrosion resistance, and excellent electric conductivity [14–17]. These characteristic properties give these materials a wider application area, including its use as cutting tools, wear proof parts, electrodes, and armor, etc. However, each of the monolithic ceramic possesses a low toughness, which limits their applications [18]. The most promising approach to toughening the ceramics is to obtain a ceramic–matrix composite by adding appropriate metallic materials into the ceramics. Titanium should be the best toughener in the titanium boride ceramics due to its high toughness, similar density and thermal expansion coefficient with boride ceramics, and excellent interfacial bonding with TiB matrix [19,20].

Considerable research has been carried out on the Ti–TiB composites with TiB up to about 30 vol%, using techniques such as casting, vacuum arc remelting, powder metallurgy, combustion synthesis, rapid solidification processing, and direct laser cladding [20–27]. Limited data is available on the microstructures and mechanical properties of the Ti–TiB composites with high volume fraction of TiB [28,29]. Furthermore, fabrication of the Ti–TiB composites containing high volume fraction of TiB by SPS technique had not yet been reported. The primary goal of the present work is to synthesize a new Ti–TiB ceramic–matrix composite containing high volume fraction of TiB, using less expensive precursors such as Ti and TiB_2 powders by SPS, and to investigate the microstructures and the mechanical properties of the *in situ* synthesized Ti–TiB composites.

2. Experimental procedures

2.1. Starting powders

The commercially available Ti powders (Mengtai Powder Business Department, Beijing, China) and TiB_2 powders (Ningxia Machinery Research Institute, Ningxia, China) were used in this procedure. The average particle size of Ti and TiB_2 powders is 30 μm and 4.5 μm, respectively. The chemical compositions of the Ti and TiB_2 powders are summarized in Tables 1 and 2, respectively. Mixtures of the composite were prepared by milling 60 wt% Ti and 40 wt% TiB_2 powders in a planetary mill for 5 h at the milling rotation speed of 300 rpm. The ethanol and agate balls were used as a milling medium. The weight ratio of balls to powder was fixed to 10:1. The resultant

* Corresponding author. Tel.: +86 10 68912709; fax: +86 10 68913951.
E-mail address: zhang@bit.edu.cn (Z.-h. Zhang).

0925-8388/$ – see front matter © 2010 Elsevier B.V. All rights reserved.
doi:10.1016/j.jallcom.2010.04.218

Table 1
Chemical compositions of the Ti powders.

Elements	α-Ti	O	N	C	Fe	H
Content (wt%)	≮ 99.7	≯ 0.08	≯ 0.06	≯ 0.04	≯ 0.08	≯ 0.04

Table 2
Chemical compositions of the TiB_2 powders.

Elements	Ti	B	O	N	C	Fe
Content (wt%)	≮ 68.5	≮ 30.9	≯ 0.35	≯ 0.02	≯ 0.12	≯ 0.10

slurry was dried in vacuum evaporator. Fig. 1 presents the SEM observations of the powder mixture.

2.2. SPS process

SPS process was performed using a pressing die made of graphite (Sanye Carbon Group, Beijing, China). The external and internal diameters of the die are 80 mm and 40 mm, respectively. DR.SINTER type SPS-3.20 equipment (Sojitz Machinery Corporation, Tokyo, Japan) with pulse duration of 3.3 ms was used. The temperature was measured by infrared thermometer. The applied initial and holding compressive pressure levels were 1 MPa and 50 MPa, respectively. The selected sintering temperatures were 1100 °C, 1200 °C, 1300 °C, and 1400 °C, with a heating rate of 150 °C/min. After soaking the powder at a desired temperature for 5 min, the applied current was reduced, the pressure was released, and the specimen was cooled to room temperature in the furnace.

2.3. Characterization tests

The diameter and height of the sintered compacts were about 40 mm and 10 mm, respectively. To avoid any contamination from graphite die, a thin layer (0.5 mm) of sintered material was removed from the surfaces of the bulk compacts before they were subjected to microstructure or property characterization.

The characteristic curves describing the relation between displacements and the sintering parameters were provided by the SPS output system. The bulk density was measured by the Archimedes method. Microstructure of the sintered materials was evaluated by SEM (Hitachi S-4800, Hitachi, Japan). Micro-hardness of the specimens was tested by micro-hardness tester (LM700AT, LECO Corporation, St. Joseph, MI) under 4.9 N. An X-ray diffraction (XRD) analysis was performed to identify the reaction products on the polished samples using an X-ray diffractometer (X'Pert PRO MPD, PANalytical B.V., Netherlands), with Cu Kα radiation. The samples were cut to various sizes for mechanical property tests with an electrical discharge saw. The bending strength (σ_b) was evaluated by three-points bending method using an Instron instrument on 3 mm × 4 mm × 36 mm specimens, with a crosshead speed of 0.5 mm/min. The tensile edges were beveled and the tensile surfaces were polished with 1 μm diamond paste. Using the same Instron equipment, fracture toughness (K_{IC}) was studied by the single-edge notched beam (SENB) method on notched 2 mm × 4 mm × 20 mm specimens, with a crosshead speed of 0.05 mm/min. Six specimens were tested for each experimental condition.

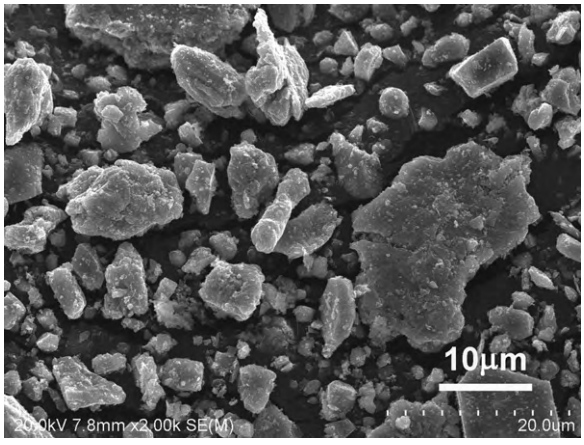

Fig. 1. SEM observations of the powder mixture.

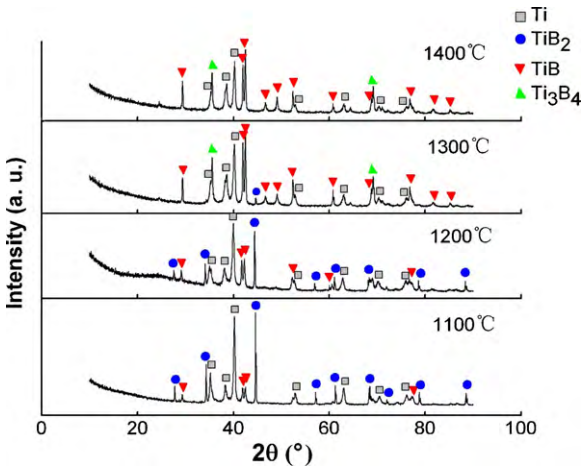

Fig. 2. XRD spectra of the Ti–TiB composites sintered at different temperatures.

3. Results and discussion

3.1. Reaction products

The reaction products of the sintered samples were first subjected to XRD analysis to identify the reaction mechanisms. The results are shown in Fig. 2. It is clear that the phases of the specimens change with the increase of the sintering temperatures, as observed from the diffraction peaks of Ti, TiB, TiB_2, and Ti_3B_4 indexed in the spectra. The diffraction peaks of Ti and TiB are present in all these spectra and the diffraction peak of Ti_3B_4 appeared in the spectra for the composite sintered at 1300 °C and 1400 °C. No diffraction peak of TiB_2 is observed in the XRD spectra for the composite sintered at 1400 °C. Moreover, the diffraction peaks of the constituent phases indexed in the spectra for the composites have no obvious change with sintering temperature rising from 1300 °C to 1400 °C, indicating that the chemical reactions were mainly completed as the sintering temperature reaches 1300 °C. The XRD spectra for the composites also suggest that the composite sintered at 1400 °C consist of Ti, TiB, and Ti_3B_4 phases. In addition, the relative volume fractions of the composition phases can be computed from the integrated intensities of the selected peaks in the X-ray diffraction pattern by the direct comparison method [30]. The results indicate that the volume fraction of TiB in the composite sintered at 1400 °C was 0.58 and that for Ti and Ti_3B_4 phases were 0.35 and 0.07, respectively.

The above mentioned results indicate that the chemical reactions shown in Eqs. (1) and (2) took place during the SPS process:

$$Ti + TiB_2 \rightarrow 2TiB \quad (1)$$

$$2TiB + TiB_2 \rightarrow Ti_3B_4 \quad (2)$$

In the sintering process, as the sintering temperature reaches 1000 °C, the chemical reaction shown in Eq. (1) took place [29]. Thus, the diffraction peak of TiB is presented in the spectra for the composite sintered at 1100 °C. With increasing sintering temperature, the volume fraction of TiB in the composites becomes more and more, whereas the volume fraction of TiB_2 and Ti in the composites decreases. As the sintering temperature exceeds 1200 °C, the reaction shown in Eq. (2) took place, leading the diffraction peak of Ti_3B_4 appear in the spectra for the composite sintered at 1300 °C. Brodkin et al. had reported that TiB can react with TiB_2 to form the plate-like Ti_3B_4 according to Eq. (2) at the soaking temperature of 1600 °C [31]. In SPS process, the local temperature in reactants particles is higher than the average sintering temperature, thus the reaction between TiB and TiB_2 had taken place as the sintering temperature reaches 1300 °C. Therefore, small quan-

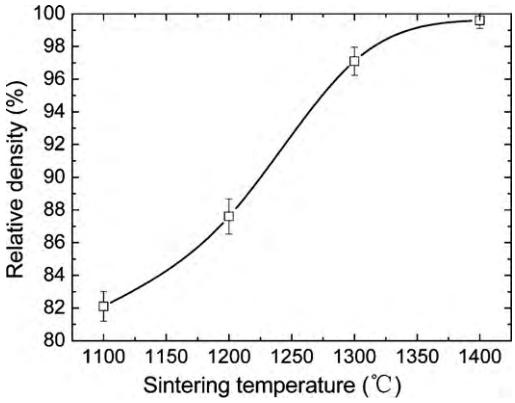

Fig. 3. Influence of sintering temperature on relative density.

tity of Ti_3B_4 was formed in the reaction products at the sintering temperature of 1300 °C and 1400 °C.

3.2. Relative density

Fig. 3 presents the curves of sintering temperature versus relative density of the sintered Ti–TiB composites. The plots reveal that the sintering temperature has remarkable influence on the relative density of the composites. With sintering temperature rising from 1100 °C to 1400 °C, the relative density of the bulk compact increases from 82.5% to 99.6%, with much of the densification occurring by the time the temperature reaches 1200 °C. As the sintering temperature exceeds 1300 °C, the density continues to increase, but at a slower rate.

3.3. Microstructure characteristics

Fig. 4 exhibits the fracture surfaces of the Ti–TiB composites obtained at different sintering temperatures. Large pores can be observed on the fracture surface of the composites sintered at 1100 °C and 1200 °C, and the porosity of the composites decreases with increasing sintering temperatures. Few pores can be detected on the fracture surface of the composites sintered at 1400 °C. Correspondingly, the relative density of the composites obtained at this temperature reaches 99.6%.

Fig. 4c and d reveals that the isolated Ti phase uniformly distributed in the *in situ* synthesized TiB matrix, and the uniformly distributed Ti phase on the fracture surface of the Ti–TiB ceramic–matrix composites shows a fractograph with dimple and quasi-cleavage, leading to an increase in fracture toughness of the composites.

The fundamental building block of TiB is the trigonal prism with the B atom at the center and the Ti atoms in corners. The orthorhombic unit cell is formed by the transverse stacking of the trigonal prisms in columnar arrays connected only at their edges (Fig. 5a). This stacking leads to a zig-zag chain of B atoms along the [0 1 0] direction with the atomic structure at the base as shown in Fig. 5b. The crystal structure of TiB shows very high asymmetry, suggesting that TiB will grow in anisotropy and form crystal with angular, planar facets. The projects of TiB along [0 1 0] and [0 0 1] directions are shown in Fig. 5c and d, respectively. They show that configuration of boron and titanium atoms are different between (0 1 0) and (0 0 1) planes. On the (0 1 0) and (0 0 1) planes, the atom ratio between titanium and boron is 1:1. However, in the (1 0 0) plane, boron atom and titanium atom occupy the sites alternating planes. The growth normal to planes containing both Ti and B atoms in the same stoichiometry as the crystal should be faster than the growth along directions involving alternating planes of Ti and B atoms. So the growth normal to plane (0 1 0) and (0 0 1) should be faster than the growth normal to plane (1 0 0). Moreover, the stacking period of atomic plane in [0 1 0] direction is shorter than that in [0 0 1] direction. The growth along [0 1 0] direction should be faster than [0 0 1] direction. So TiB is likely to grow along [0 1 0] direction and form whisker shape [32–34]. Fig. 6 presents the fracture surfaces of the Ti–TiB composites sintered at 1100 °C and 1200 °C at high magnification, indicating that the *in situ* synthesized TiB was lath-like shaped and uniformly distributed along the Ti phase boundaries. Fig. 7 presents the fracture surfaces of the Ti–TiB com-

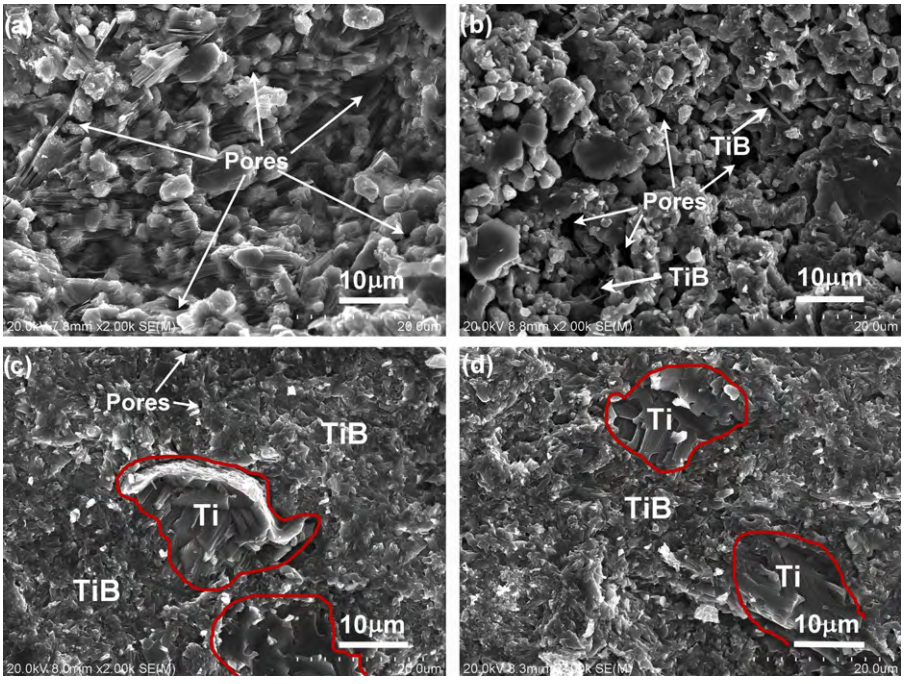

Fig. 4. SEM images showing the fracture surface of the Ti–TiB composites sintered at temperatures of: (a) 1100 °C, (b) 1200 °C, (c) 1300 °C, and (d) 1400 °C.

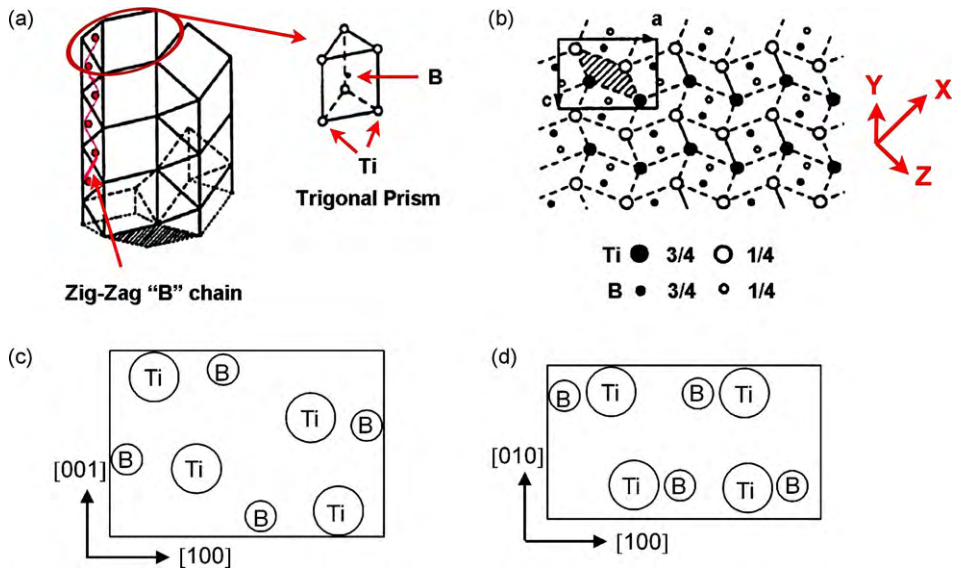

Fig. 5. Crystal structure of TiB: (a) the stacking of the trigonal prisms with zig-zag B chain, (b) the close packing of the prism, (c) project along the [0 1 0] direction, and (d) project along the [0 0 1] direction.

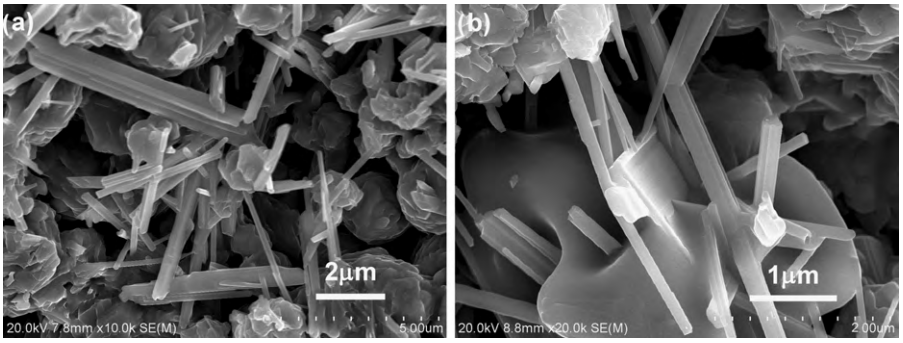

Fig. 6. High magnification SEM images showing fracture surface of the composites sintered at temperatures of: (a) 1100 °C and (b) 1200 °C.

posites sintered at 1300 °C and 1400 °C at high magnification. Since the chemical reactions were mainly completed as the temperature reaches 1300 °C, the TiB whiskers and the remaining Ti were then responsible for the further consolidation process. With increasing sintering temperature, the resulting TiB whiskers grew and connected rapidly; making TiB whiskers coarsen and agglomerate obviously.

3.4. Mechanical properties

Fig. 8 presents the curves of sintering temperature versus micro-hardness of the sintered Ti–TiB composites. The plots reveal that the micro-hardness of the composites increases with rising sintering temperature. When sintered at 1400 °C, the average micro-hardness of the composite reaches 18.3 GPa, which is close to the hardness (19 GPa) of the monolithic TiB ceramic with full density [35].

Fig. 9 shows the influence of sintering temperature on bending strength and fracture toughness of the Ti–TiB composites. With rising sintering temperature, both the bending strength and the fracture toughness increase. When sintered at 1100 °C, the bending strength and the fracture toughness of the composite are 285 MPa, 6.71 MPa $m^{1/2}$, respectively. By comparison, the composite sintered at 1400 °C has the highest bending strength of 608 MPa and the

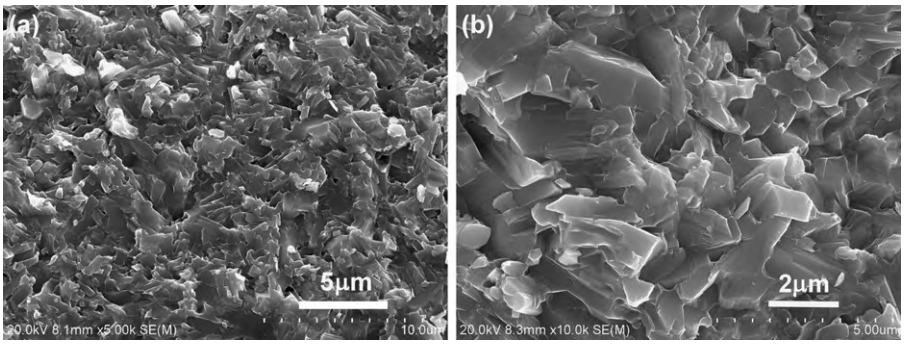

Fig. 7. High magnification SEM images showing fracture surface of the composites sintered at temperatures of: (a) 1300 °C and (b) 1400 °C.

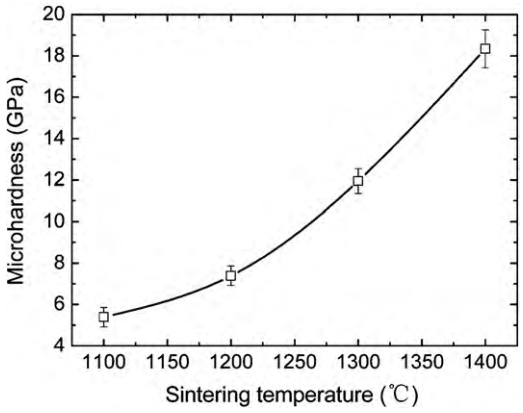

Fig. 8. Micro-hardness of the composites sintered at different temperatures.

highest fracture toughness of 9.35 MPa $m^{1/2}$. In addition, both the bending strength and the fracture toughness of the Ti–TiB composite synthesized by SPS technique at sintering temperature of 1400 °C are greater than that (360 MPa, 4.5 MPa $m^{1/2}$, respectively) of the monolithic TiB ceramic with full density.

The relative density and grain size have obvious influence on the bending strength of ceramic materials. Usually, the bending strength increases with increasing relative density and decreasing grain size. For Ti–TiB ceramic–matrix composites synthesized by SPS process, the grain growth is prohibited effectively by reducing sintering temperature and sintering time due to the high heating rate and the efficient heat transfer [36,37]. Therefore, the bending strength of the Ti–TiB ceramic–matrix composites is mainly determined by the relative density. Thus, rise in the sintering temperature can increase the bending strength remarkably due to the increase of the density.

Fracture toughness is a property that materials resist to the propagation of cracks. Increase of sintering temperature makes the Ti–TiB ceramic–matrix composites more dense, porosity decreases, hence the fracture toughness increases. Moreover, the fine and lath-shaped grains lead to much more grain boundaries, which can impede the propagation of cracks by the mechanism of crack deflection with absorbing much energy of micro-crack expansion. Additionally, the presented dimple and quasi-cleavage fracture of the Ti grains, pull-out and the micro-fracture of lath-shaped TiB grains on the fracture surface of the Ti–TiB composites also absorb much energy of micro-crack expansion. Thus, the fracture toughness of the Ti–TiB ceramic–matrix composites synthesized by SPS technique is improved remarkably due to the dimple and quasi-cleavage fracture of Ti grains, crack deflection, pull-out and the micro-fracture of lath-shaped TiB grains.

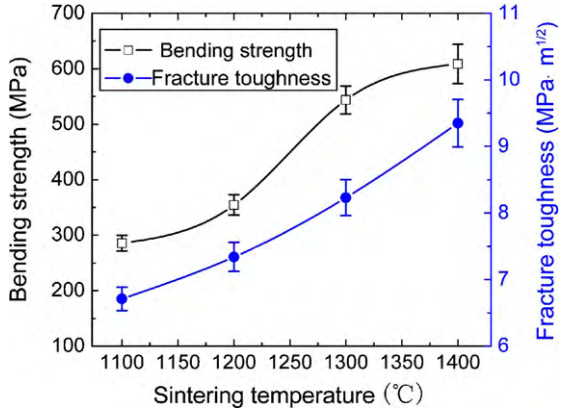

Fig. 9. Bending strength and fracture toughness of the composites sintered at different temperatures.

4. Conclusions

Bending strength, fracture toughness and hardness are the most important mechanical properties of the ceramics and ceramic–matrix composites for advanced engineering and military applications. Unfortunately, these targets usually cannot be satisfied simultaneously, especially hardness and fracture toughness are often mutually exclusive; ceramics and ceramic–matrix composites may be hard or tough but are rarely both. In the present study, Ti–TiB ceramic–matrix composites were *in situ* synthesized by SPS process with optimized sintering parameters. Compared with the monolithic TiB and TiB_2 ceramic, the Ti–TiB composite synthesized by SPS process at sintering temperature of 1400 °C have higher bending strength (608 MPa) and fracture toughness (9.35 MPa $m^{1/2}$). In addition, the hardness of the composite maintains a fairly high level (18.3 GPa). Due to the excellent comprehensive mechanical properties, the *in situ* synthesized Ti–TiB ceramic–matrix composites by SPS technique constitutes a wonderful choice for applications in high performance cutting tools and abrasives, wear resistant parts, especially in all kinds of armored vehicles.

Acknowledgements

The authors wish to thank Dr. Yunfei Xue and Dr. Linda Wang for their contributions to the investigation. The study was supported by the Program for Peking Excellent Talents in the University under Grant Number 20061D0503200316, and the National Defense Pre-Research Foundation of China under Grant Number of 9140A12050209BQ0137.

References

[1] R. Licheri, R. Orrù, C. Musa, A.M. Locci, G. Cao, J. Alloys Compd. 478 (2009) 572–578.
[2] J.S. Kim, I.V. Povstugar, P.P. Choi, E.P. Yelsukov, Y.S. Kwon, J. Alloys Compd. 486 (2009) 511–514.
[3] Z.H. Zhang, F.C. Wang, S.K. Lee, Y. Y. Liu, J.W. Cheng, Y. Liang, Mater. Sci. Eng. A 523 (2009) 134–138.
[4] P. Angerer, J. Wosik, E. Neubauer, L.G. Yu, G.E. Nauer, K.A. Khor, Int. J. Refract. Met. Hard Mater. 27 (2009) 105–110.
[5] X.L. He, F. Ye, Z.Q. Zhou, H.J. Zhang, J. Alloys Compd. 496 (2010) 413–417.
[6] J.H. Chae, K.H. Kim, Y.H. Choa, J.I. Matsushita, J.W. Yoon, K.B. Shim, J. Alloys Compd. 413 (2006) 259–264.
[7] Z.H. Zhang, F.C. Wang, J. Luo, S.K. Lee, L. Wang, Mater. Sci. Eng. A 527 (2010) 2099–2103.
[8] R. Kumar, K.H. Prakash, Acta Mater. 53 (2005) 2327–2335.
[9] F. Monteverde, J. Alloys Compd. 428 (2007) 197–205.
[10] Z.H. Zhang, F.C. Wang, S.K. Li, M.W. Shen, S. Osamu, Mater. Charact. 59 (2008) 329–333.
[11] M. Kubota, J. Alloys Compd. 434–435 (2007) 294–297.
[12] M. Kubota, P. Cizek, J. Alloys Compd. 457 (2008) 209–215.
[13] A. Singh, S.P. Harimkar, J. Alloys Compd. 497 (2010) 121–126.
[14] A. Jain, R. Pankajavalli, S. Anthonysamy, K. Ananthasivan, R. Babu, V. Ganesan, G.S. Gupta, J. Alloys Compd. 491 (2010) 747–752.
[15] G.J. Cao, L. Geng, M. Naka, J. Am. Ceram. Soc. 89 (2006) 3836–3838.
[16] S. Madtha, C. Lee, K.S. Ravi-Chandran, J. Am. Ceram. Soc. 91 (2008) 1319–1321.
[17] K.B. Panda, K.S. Ravi-Chandran, Acta Mater. 54 (2006) 1641–1657.
[18] F.C. Wang, Z.H. Zhang, J. Luo, C.C. Huang, S.K. Lee, Compos. Sci. Technol. 69 (2009) 2682–2687.
[19] H.B. Feng, Y. Zhou, D.C. Jia, Q.C. Meng, Compos. Sci. Technol. 64 (2004) 2495–2500.
[20] J.Q. Lu, J.N. Qin, Y.F. Chen, Z.W. Zhang, W.J. Lu, D. Zhang, J. Alloys Compd. 490 (2010) 118–123.
[21] J.Q. Lu, J.N. Qin, W.J. Lu, D. Zhang, H.L. Hou, Z.Q. Li, Mater. Sci. Eng. A 500 (2009) 1–7.
[22] J.Q. Lu, J.N. Qin, W.J. Lu, Y. Liu, J.J. Gu, D. Zhang, J. Alloys Compd. 469 (2009) 116–122.
[23] C.J. Boehlert, S. Tamirisakandala, W.A. Curtin, D.B. Miracle, Scripta Mater. 61 (2009) 245–248.
[24] X.H. Zhang, Q. Xu, J.C. Han, V.L. Kvanin, Mater. Sci. Eng. A 348 (2003) 41–46.

[25] M.M. Wang, W.J. Lu, J.N. Qin, D. Zhang, B. Ji, F. Zhu, Scripta Mater. 54 (2006) 1955–1959.
[26] S.I. Lieberman, A.M. Gokhale, S. Tamirisakandala, R.B. Bhat, Mater. Charact. 60 (2009) 957–963.
[27] J. Duttamajumdar, L. Li, Mater. Lett. 64 (2010) 1010–1012.
[28] J.P. Quast, C.J. Boehlert, R. Gardner, E. Tuegel, T. Wyen, Mater. Sci. Eng. A 497 (2008) 1–9.
[29] X.H. Zhang, L. Xu, S.Y. Du, C.Y. Liu, J.C. Han, W.B. Han, J. Alloys Compd. 466 (2008) 241–245.
[30] S.S. Sahay, K.S. Ravichandran, R. Arti, J. Mater. Res. 14 (1999) 4214–4223.
[31] D. Brodkin, S.R. Kalidindi, M.W. Barsoum, A. Zavaliangos, J. Am. Ceram. Soc. 79 (1996) 1945–1952.
[32] H.B. Feng, Q.C. Meng, Y. Zhou, D.C. Jia, Mater. Sci. Eng. A 397 (2005) 92–97.
[33] W.J. Lu, D. Zhang, X.N. Zhang, R.J. Wu, T. Sakata, H. Mori, J. Alloys Compd. 327 (2001) 240–247.
[34] B.J. Kooi, Y.T. Pei, J.Th.M. De Hosson, Acta Mater. 51 (2003) 831–845.
[35] S. Nakane, Y. Takano, M. Yoshinaka, K. Hirota, O. Yamaguchi, J. Am. Ceram. Soc. 82 (1999) 1627–1628.
[36] Z.H. Zhang, F.C. Wang, L. Wang, S.K. Li, Mater. Lett. 62 (2008) 3987–3990.
[37] T.T. Sasaki, T. Ohkubo, K. Hono, Acta Mater. 57 (2009) 3529–3538.